Accepted Manuscript

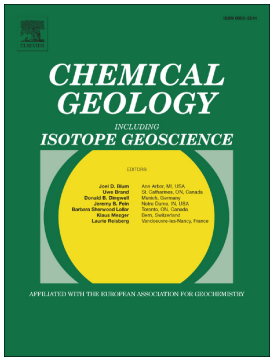


# Silicate-sulfide liquid immiscibility in modern arc basalt (Tolbachik volcano, Kamchatka): Part I. Occurrence and compositions of sulfide melts

M. Zelenski, V.S. Kamenetsky, J.A. Mavrogenes, A.A. Gurenko, L.V. Danyushevsky

PII: S0009-2541(17)30514-4
DOI: doi: 10.1016/j.chemgeo.2017.09.013
Reference: CHEMGE 18468

To appear in: *Chemical Geology*

Received date: 25 April 2017
Revised date: 21 July 2017
Accepted date: 11 September 2017

Please cite this article as: M. Zelenski, V.S. Kamenetsky, J.A. Mavrogenes, A.A. Gurenko, L.V. Danyushevsky , Silicate-sulfide liquid immiscibility in modern arc basalt (Tolbachik volcano, Kamchatka): Part I. Occurrence and compositions of sulfide melts, *Chemical Geology* (2017), doi: 10.1016/j.chemgeo.2017.09.013

# Silicate-sulfide liquid immiscibility in modern arc basalt (Tolbachik volcano, Kamchatka): Part I. Occurrence and compositions of sulfide melts.

M. Zelenski [a], V.S. Kamenetsky [b,a*], J.A. Mavrogenes [c], A.A. Gurenko [d], L.V. Danyushevsky [b,e]

[a] *Institute of Experimental Mineralogy RAS, Chernogolovka 142432, Russia*
[b] *CODES and Earth Sciences, University of Tasmania, Private Bag 79, Hobart, TAS 7001, Australia*
[c] *Research School of Earth Sciences, Australian National University, Canberra, ACT 2601, Australia*
[d] *Centre de Recherches Pétrographiques et Géochimiques (CRPG), UMR 7358, Université de Lorraine, 54501 Vandoeuvre-lès-Nancy, France*
[e] *ARC TMVC Research Hub, University of Tasmania, Private Bag 79, Hobart, TAS 7001, Australia*

* Corresponding author at: School of Physical Sciences, University of Tasmania, Hobart, TAS 7001, Australia.
*E-mail address*: Dima.Kamenetsky@utas.edu.au (V. Kamenetsky).

Keywords: Sulfide, immiscibility, olivine, melt inclusions, chalcophile metals, island-arc magma, Tolbachik volcano

ABSTRACT

Silicate-sulfide liquid immiscibility plays a key role in the formation of magmatic sulfide ore deposits but incipient sulfide melts are rarely preserved in natural rocks. This study presents the distribution and compositions of olivine-hosted sulfide melt globules resulting from silicate-sulfide liquid immiscibility in primitive arc basalts. Abundant sulfide droplets entrapped in olivine from primitive basalts of the 1941 eruption and pre-historic eruptive cone "Mt. 1004" of the Tolbachik volcano, Kurile-Kamchatka arc. Inclusions range from submicron to 250 μm in size, coexist with sulfur-rich glass (≤ 1.1 wt% S), and, in some cases, with magmatic anhydrite. Saturation in sulfide occurred early in the evolution of a water- and sulfur-rich magma, moderately oxidized (QFM+1…+1.5), which crystallized high-Mg olivine ($Fo_{86-92}$), clinopyroxene and Cr-spinel. The process developed dense "clouds" of sulfide in relatively small volumes of magma, with highly variable abundances of chalcophile metals. The low degree of sulfide supersaturation promoted diffusive equilibration of the growing droplets with the melt in Ni and Cu, resulting in high concentrations (≈38 mol%) of CuS and NiS in the earliest sulfide liquids. The Tolbachik samples provide a glimpse into deep arc processes not seen elsewhere, and may show how arc magmas, despite their oxidized nature, saturate in sulfide.

## 1. Introduction

Immiscible sulfide melt segregates from silicate melt if the concentration of $S^{2-}$ (sulfide) in the silicate melt surpasses the sulfur content at sulfide saturation (SCSS, e.g. Li and Ripley, 2005; O'Neill and Mavrogenes, 2002; Wykes et al., 2014). Chalcophile and highly siderophile elements (Cu, Ni, Au, PGE etc.) are present in the silicate melt in low concentrations but strongly partition into sulfide, such that even small amounts of sulfide melt collect most or all of the chalcophile elements. Because of its high specific gravity, sulfide melt tends to accumulate in lower parts of magma chambers, which become potential Cu-Ni-(PGE) magmatic sulfide ore deposits (e.g. Naldrett, 2004). The phenomenon of sulfide-silicate immiscibility plays a key role in the formation

of magmatic sulfide ores and has been extensively studied, both experimentally (e.g. Holzheid, 2010; Jugo et al., 2005a; Jugo et al., 2005b; Jugo et al., 2010; Namur et al., 2016; O'Neill and Mavrogenes, 2002; Peach and Mathez, 1993; Smythe et al., 2017) and theoretically (e.g. Ariskin et al., 2013; Mungall, 2002; Zhang, 2015). Micron-sized sulfide droplets and silicate melt inclusions containing sulfides are occasionally found in quenched underwater glasses or early magmatic phases grown from primitive melts in oceanic rifts and intraplate oceanic settings (e.g. Ackermand et al., 1998; Czamanske and Moore, 1977; Francis, 1990; Gurenko et al., 1987; Kamenetsky et al., 2013; Mathez, 1976; Patten et al., 2012; Peach et al., 1990; Stone and Fleet, 1991).

Although arc basaltic magmas are often sulfur-rich (Wallace and Edmonds, 2011) and therefore could potentially form sulfides, they are commonly more oxidized than mid-ocean ridge and intraplate oceanic basalts (e.g. Evans et al., 2012; Richards, 2015 and references therein), within the range of $fO_2$ from QFM+1 to QFM+3 for the majority of samples (see review in Matjuschkin et al., 2016 and references therein). Since at $fO_2$ > QFM+1 sulfur exists primarily as sulfate (e.g. Jugo et al., 2005a; Jugo et al., 2010), arc basalts are not expected to saturate in sulfide unless they are reduced by graphite or other reductants from assimilated country rocks (Tomkins et al., 2012) or via $SO_2$ reactions with calcic host rocks (Henley et al., 2015; Mavrogenes and Blundy, 2017). An exception is Cu-Fe sulfides trapped as inclusions in minerals in evolved arc magmas (e.g. Humphreys et al., 2015; Nadeau et al., 2010, and references therein), due either to a change in volatile content (Humphreys et al., 2015) or magnetite crystallization (Jenner et al., 2010). Such sulfides are typically Cu-rich, Ni- and PGE-poor and never form large accumulations unlike early Ni-PGE-rich magmatic sulfides from Mg-rich primitive melts (Naldrett, 2004). Moreover, direct evidence of incipient sulfide melts in continental settings is partially or completely eradicated by oxidation of sulfide melts and their crystalline products by magmatic and deuteric fluids (e.g. Keith et al., 1997; Larocque et al., 2000; Wilkinson, 2013).

This study of micron-sized sulfide globules in olivine phenocrysts from Tolbachik volcano, Kurile-Kamchatka arc investigates the timing of sulfide saturation and compositions of immiscible sulfide melts. We show that sulfide saturation occurred early in primitive magmas and persisted during olivine crystallization. We also discuss triggers for sulfide saturation in this particular case, and make implications for sulfide melt evolution and entrapment into olivine phenocrysts.

## 2. Tolbachik volcano and rocks

The Tolbachik Volcanic Complex in the central part of the Central Kamchatka Depression (CKD) is the southernmost of the Klyuchevskoy Group of volcanoes, which is located at the north end of the Kurile-Kamchatka arc close to Kamchatka-Aleutian arc junction. Volcanism at Kamchatka is driven by the subducting Pacific Plate, which moves in NW direction at ~80 mm/year (DeMets et al., 1990; Steblov et al., 2003). The subducting plate is relatively cold with estimated age of ~90 Ma (Gorbatov et al., 1997). The depth of the Moho discontinuity beneath Tolbachik was estimated at 30-42 km, with uncertainties due to "a gradual transition from crustal to upper-mantle rocks" (Iwasaki et al., 2013 and references therein). The depth to the Benioff zone under Tolbachik is ~180 km (Gorbatov et al., 1997). Three volcanoes of the Klyuchevskoy Group (Tolbachik, Klyuchevskoy and Shiveluch) each ejected around 2 $km^3$ of lava and tephra in dense-rock equivalent during the last 80 years (time of observations), which makes these volcanoes the most productive arc volcanoes on Earth (Portnyagin et al., 2005). A combination of mantle upwelling coupled with decompression melting and fluid-triggered melting of the mantle wedge was proposed to explain anomalously high productivity of Tolbachik and other volcanoes in the CKD (Portnyagin et al., 2005).

The Tolbachik complex consists of the Ostry Tolbachik stratovolcano (extinct), the Plosky Tolbachik stratovolcano (active) and two chains of more than 170 monogenetic scoria cones and associated lava fields that extend NE and SSW from Plosky Tolbachik (Fig. 1, Supplementary Fig. S1). Plosky Tolbachik is renowned for its voluminous effusive eruptions of low-viscosity magmas. A detailed literature review of the lithospheric structure and tectonic setting of the region can be found in Churikova et al. (2015a) and Portnyagin et al. (2007a). A recent review of the magmatic

system of Tolbachik volcano was presented by Belousov et al. (2015). Chemical compositions and petrographic features of Tolbachik rocks can be found in published literature (e.g. Churikova et al., 2015a; Churikova et al., 2015b; Flerov et al., 1984; Portnyagin et al., 2007a; Portnyagin et al., 2015).

Tolbachik rocks vary from basalts to basaltic trachyandesites (Supplementary Fig. S2a) and have a bimodal distribution of MgO, ranging from 3 to 5.5 wt% MgO (low-Mg basaltic trachyandesites) and from 8 to 11.5 wt% MgO (high-Mg basalts) (Supplementary Fig. S2b). High-Al basalts make up more than 90% of the total ejected material. High-Mg basalts are thought to represent near primary arc magmas and are among the most primitive arc rocks globally (Portnyagin et al., 2007a). Both high- and low-Mg Tolbachik rocks belong to either medium-K or high-K rock series (Supplementary Fig. S2b). The existence of the high-K series was attributed to mantle upwelling due to intra-arc rifting (Churikova et al., 2015b). Alternatively, the compositions of the Tolbachik volcanic series with anomalously broad range (5–8-fold) of concentrations of incompatible elements (K, Rb, Nb, Ba) at a given MgO content fits a Recharge-Evacuation-Fractional Crystallization model (Portnyagin et al., 2015). Basalts from the 1941 eruption cone and the Mt. 1004 cone are classified as high-Mg, high-K basalt (Supplementary Fig. S2b) and contain olivine phenocrysts with sulfide globules, which are the focus of this study.

## 3. Samples and Methods

The samples for this study were collected from the 1941 eruptive cone (summit at 55.7949° N, 160.3321° E, 2104 m asl), 3.5 km SW of the edge of the summit caldera of Plosky Tolbachik (Fig. 1, Supplementary Fig. S1). It is a ~100 m high scoria cone with a 5 km-long lava and an adjacent field covered by volcanic bombs and scoria (Supplementary Fig. S2), with a total volume of ejected basaltic material of ~ 0.07–0.10 $km^3$ (Braitseva et al., 1984; Piip, 1946). The samples included three scoria samples, each of about 10 kg; two samples of compact lava and two samples of volcanic bombs, altogether more than 60 kg. Scoria and bomb samples were collected ~ 200 m apart of each other (Supplementary Table S1), but did not reveal any difference in bulk rock composition and sulfide abundances. The 1941 magnesian basalts (50.5-51.0% $SiO_2$ and 8.9% MgO; Supplementary Table S2) contain ~4 wt% phenocrysts of olivine, the majority of which are 1-5 mm crystals (85–91 mol% Fo; Fig. 2). In addition to olivine, the rock contains rare plagioclase and pyroxene phenocrysts. The groundmass comprises clinopyroxene, plagioclase, Ti-magnetite and glass.

Additional samples were from “Mt. 1004” – a pre-historic, ~ 150 m-high cone (55.6753° N, 160.2369° E) located 15 km SSW from the 1941 cone (Fig. 1). Mt. 1004 rocks are both high-alumina and high-magnesian basalts; the latter are compositionally similar to the 1941 eruption rocks, but contain more phenocrysts of olivine and clinopyroxene (up to 10 %), thus resulting in higher MgO contents (up to 11.5 wt%).

Samples of lava and scoria were crushed and sieved, followed by separation of a 0.3–1.5 mm fraction in a heavy liquid with a specific gravity of 3.0 (75% bromoform + 25% methylene iodide). The addition of methylene iodide ($\rho$=3.32) was necessary because of the high specific gravity of the rock groundmass ($\rho$~2.9–2.95) that exceeds specific gravity of pure bromoform ($\rho$=2.89). Olivine grains from the heavy fraction were placed in a Petri dish under immersion oil in a layer spread across the surface, and examined using a binocular microscope. About 1200 olivine grains containing sulfide globules were found among ~ 200,000 examined grains. Only crystals with large sulfide globules (≥ 20 μm) and sulfide “swarms” were selected for further studies. Several tens of sulfide-bearing olivine grains were mixed with a 5 μm powder of SiC and diamond (to maintain reductive atmosphere in an ampoule), placed in the Pt ampoule 2.5 mm in diameter, heated in a vertical furnace at 1200 °C for 5 minutes, followed by rapid quenching (~500 °C/s) in water. Heating was aimed at rehomogenization of sulfides and making their analyzed compositions more representative of the trapped sulfide liquid.

Both unheated and heated sulfide globules were exposed and polished using 1μm diamond paste and studied by scanning electron microscopy with energy-dispersive spectrometer (Vega Tescan II XMU, Institute of Experimental Mineralogy, Russian Academy of Sciences,

Chernogolovka, Russia; Hitachi SU-70, Central Science Laboratory, University of Tasmania, Hobart). Major and trace element contents in rock samples were analyzed by XRF and ICP-MS in commercial Geoscience Laboratories, Sudbury, Ontario. Concentrations of major elements, S and Cl in vitreous melt inclusions were measured using electron microprobe microanalyzer with WDS detectors Cameca SX-100 (Institute of Geochemistry and Analytical Chemistry, Russian Academy of Sciences, Moscow). Analytical conditions were 15 kV accelerating voltage and 12 nA probe current with a 10 μm defocused spot and counting time of 20–60 s; matrix effects were corrected using the ZAF method. The analytical conditions and instrumentation used for laser ablation ICPMS analysis of sulfide-bearing olivine and sulfide globules are presented in the Supplementary Materials and the companion paper (Kamenetsky et al., 2017).

## 4. Results

### *4.1. Olivine phenocrysts and olivine-hosted inclusions*

Studied olivine phenocrysts are loose crystals in tephra with little basaltic glass attached to their surface, crystals from thick basalt flows and scoria bombs. The olivine grains, belonging to different eruptive (magma fragmentation) modes, underwent cooling at different rates, from rapid (loose crystals) through intermediate (in tephra and bombs) to slow (lava). Most crystals show normal zoning from cores of $Fo_{88-92}$ to rims of $Fo_{82-85}$ with most compositions between 88 and 91 mol% Fo (Fig. 2). Olivine phenocrysts contain numerous inclusions of crystals (Cr-spinel, clinopyroxene and orthopyroxene), silicate melt (glassy to partly crystallized), fluid bubbles, sulfide globules and combinations of the above phases in random proportions (Kamenetsky et al., 2017). Compositions of olivine, hosting silicate and sulfide melt inclusions, are detailed in Kamenetsky et al. (2017). The abundances of Ni and Cu in olivine grains containing sulfide inclusions (Fig. 2b-d; Supplementary Table S3) are of particular interest, as they may reflect the concentration of these chalcophile metals in the magma undergoing sulfide immiscibility. In the sulfide-free olivine phenocrysts the abundance of Ni is positively correlated with Fo (2900 to 1200 ppm in $Fo_{91-87}$), whereas Cu remains almost constant (3.2 ± 0.5 ppm). In contrast, the olivine phenocrysts with sulfide inclusions are characterized by variable and systematically lower Ni and scattered Cu (0.7-6.6 ppm) contents at a given Fo (Fig. 2b-d).

Compositions of silicate melt inclusions, corrected for in-situ olivine crystallization, are more primitive, but still overlap with the whole rock MgO (6-13 and 8.9 wt%, respectively) contents (Kamenetsky et al., 2017). However, the compositions of melt inclusions and host basalts cannot be linked by simple fractional crystallization of common phenocrysts, as the abundances of $K_2O$ (0.50-0.85 and 1.35 wt%, respectively), as well as $P_2O_5$ and trace element ratios (e.g. Sr/Nd, Ba/Rb, Zr/Hf, Zr/Sm etc.) are principally different. Volatile contents in glass from such melt inclusions vary from near zero to exceptionally high values, originally containing at least 5.2 wt% $H_2O$, 1200 ppm $CO_2$ and 0.28 wt% Cl (Kamenetsky et al., 2017). Naturally quenched melt inclusions are characterized by high S abundances (up to 0.30–0.35 wt%, Fig. 3). Some melt inclusions, especially those associated with sulfides and/or containing anhydrite (Fig. 3, 5a-d, h), are even more enriched in sulfur (up to 1.1 wt%; Supplementary Fig. S3).

### *4.2. Sulfide globules in olivine*

Approximately 0.6 % and 0.2 % of olivine grains extracted from the 1941 cone and Mt. 1004 cone samples, respectively, contain a sulfide melt inclusion (hereafter, sulfide droplet or sulfide globule), or a group of such inclusions (Fig. 4, 5). In total, ~1200 and ~ 100 grains olivine grains with sulfides were picked up from the studied samples of 1941 eruption and Mt. 1004, respectively. Most sulfide droplets are 10 to 100 microns across, rarely reaching 250 microns. Occasionally, sub-micron to micron-sized inclusions form “swarms” consisting of hundreds to thousands of individual droplets (Fig. 4a-d), with a calculated volume density exceeding 8,000 droplets/$mm^3$. Rarely, sulfides occur as inclusion arrays (Fig. 4b, f) or form thin films inside cracks in olivine (Fig. 4g).

Tolbachik sulfides occur exclusively as inclusions in olivine phenocrysts; none have been observed within the rock groundmass. Sulfide globules are commonly enclosed directly in olivine

(Fig. 5e-g), but ~ 30% have a coating of the silicate melt, with or without fluid bubbles, or reside in silicate melt inclusions (Fig. 5a-d, g). The majority of the droplets are nearly spherical, though some are flattened/elongated (Fig. 4b, f); their spherical morphology indicates they were captured as liquid. Many droplets have cavities on the surface or closed pores inside (Fig. 5c, d), or are surrounded by bubbles that probably contained aqueous fluid (Fig. 5b).

The majority of sectioned sulfide globules, especially naturally quenched (Fig. 5a, c-e) in olivine from tephra and those that were experimentally heated and quenched (Fig. 5g, h), are texturally homogeneous. Some examined sulfide globules in olivine from the lava samples appear as fine or coarse intergrowths of MSS (Fe-Ni-S monosulfide solid solution) and ISS (Fe-Cu-S intermediate solid solution) and may be also composed of crisscrossing intergrowths of chalcopyrite ($CuFeS_2$) and cubanite ($CuFe_2S_3$), associated with "patches" of mackinawite $(Fe,Ni)S_{0.9}$ or pentlandite $(Fe,Ni)_9S_8$ (Fig. 5e, f). Smaller sulfide globules (< 10 μm) tend to be always homogeneous. Given occurrence of homogeneous and inhomogeneous textures in sulfides from the tephra and lava samples respectively, we relate differences in phase compositions and textures to fast and slow cooling rates.

Average bulk compositions of individual globules were obtained by rastered beam energy-dispersive X-ray spectroscopy (EDS) collected over the exposed globule surfaces. Considering the fine-grained texture of the majority of globules, this analysis provides values close to the bulk (volume) composition even for visually heterogeneous, multiphase globules. Admittedly, the third dimension is missing from these analyses, but the representativeness of the compositions analyzed at the surface was confirmed by the LA-ICPMS analyses of selected globules, which correlated with EDS estimates (Fig. 6, Supplementary Table S3). The amount of oxygen in the Tolbachik sulfides does not exceed a few wt%, and is stored in low-Ti magnetite, which is interstitial to sulfide phases (Fig. 5e, f).

The studied sulfide droplets are characterized by an average Me:S ratio of 0.938 ± 0.075 (2σ) and 0.998 ± 0.076 (2σ) for unheated and heated samples, respectively (Supplementary Tables S3-S5). As these values are close to unity they can be presented on a FeS-NiS-CuS ternary. The majority of the compositional data is distributed within the FeS-0.6NiS-0.6CuS ternary (Fig. 7a, b). The maximum measured contents of NiS and CuS are 38.1 and 37.6 mol% respectively; the rest being FeS. Large globules tend to be enriched in Cu, whereas smaller globules in swarms are Ni-rich (Fig. 4c; Supplementary Table S4). Sulfides from the 1941 cone and from the Mt. 1004 cone are compositionally similar.

## 5. Discussion

### *5.1. Sulfide melt compositional variability*

Strong compositional variability recorded in the Tolbachik sulfide globules (Fig. 7a, b) is mirrored in the sulfide globules in glasses and phenocrysts from other tectonic settings (Fig. 7c). Among a number of chemical and physical parameters that can be responsible for compositions of incipient sulfide liquids, the abundance of chalcophile metals in the silicate melt undergoing immiscibility, is considered in our study. Unfortunately, records of metal contents in natural silicate melts prior to immiscibility do not exist; however, phenocrysts from same magmatic systems may register chemical composition and evolution of their parental magmas. In the case of studied Tolbachik magmas, the sulfide-free olivine phenocrysts document typical fractionation of Ni and Cu, whereas the composition of sulfide-bearing olivine is much more diverse (Fig. 2b-d). Significant scatter in abundances of Ni, Cu and Ni/Cu for a given Fo value of the sulfide-bearing olivine (Fig. 2b-d) testifies to similarly variable abundances of these metals and their ratio in the magma. On the other hand, the compositions of olivine and olivine-hosted sulfide inclusions are unambiguously related to abundances of chalcophile metals and their ratios (Fig. 8). Taken together with the compositional variability of olivine (Fig. 2b-d), this strongly supports the equilibrium between host olivine and trapped sulfide melts, and argues for fluctuating concentrations of chalcophile metals in parental magmas.

Another possible explanation for systematically lower Ni content in olivine with sulfide globules (Fig. 2c) is Ni equilibrium exchange between olivine and sulfide (Barnes et al., 2013). The partitioning coefficient $K_D = (NiS/FeS)_{sulfide}/(NiO/FeO)_{olivine}$ depends positively on Ni content in the sulfide melt and decreases with increasing oxygen fugacity (Fig. 9; Barnes et al., 2013). The compositional relationships between the Tolbachik sulfide globules and their host olivine suggest $fO_2$ corresponding to QFM+1 or slightly more oxidized conditions (Fig. 9). These are in agreement $fO_2$ ~ QFM + 1 ... + 1.5, deduced from the Tolbachik Cr-spinel compositions (Kamenetsky et al., 2017).

*5.2. Kinetic controls on sulfide melt compositions*

It is generally accepted that early sulfide melt forming due to silicate-sulfide immiscibility is close in composition to FeS (Naldrett, 2004; Zhang, 2015) and then interacts with sufficient amount of magma to acquire chalcophile elements. Alternatively, the model of "kinetic equilibration" (Mungall, 2002) predicts that incipient sulfide melts are not necessarily poor in chalcophile elements at low degrees of sulfide supersaturation. High concentrations of chalcophile metals can be acquired by a slow-growing sulfide melt droplet that equilibrates with a large volume of the melt containing sufficient amounts of Cu and Ni. In fact, diffusion fluxes of metals that strongly partition into FeS liquid can surpass diffusion flux of FeS, resulting in instantaneous saturation of incipient sulfide droplets in chalcophile elements. According to Fick's first law, the mass flux $J=-D\cdot(d\varphi/dx)$, where D is the diffusivity coefficient and $d\varphi/dx$ is the concentration gradient; in the case of sulfide supersaturation, only the fraction of S in the melt that exceeds the saturation level is expected to diffuse towards a growing sulfide droplet.

A rigorous solution of diffusion equations for the sulfide growth is not straightforward. However, the ratio of metal flux to $S^{2-}$ flux from a silicate melt to growing sulfide droplets can be determined through consideration of the apparent R factor, i.e., a proportion between volumes of daughter sulfide melt and parental silicate melt, which provides metallic elements. According to Mungall (2002), if a sulfide droplet is essentially static (which is the case for micron-sized droplets), then apparent R factor can be presented as:

$$R = \frac{D_{me}}{D_{FeS}} \times \frac{1}{C_0^{FeS}}$$

where $D_{(Me)}$ and $D_{(FeS)}$ are diffusivities of a metal and FeS and $C^{FeS}_0$ is the degree of sulfide supersaturation. If the concentration of $S^{2-}$ (FeS) in the melt just exceeds the saturation level, the second multiplier in the above equation approaches infinity and R factor will be high for all elements, even for those with low diffusivities. Diffusion flux of FeS to the droplet will be kinetically restricted and can be surpassed by fluxes of Cu and Ni. This probably occurred within the studied Tolbachik magmas, resulting in very high contents (30-38 mol%) of NiS and CuS even in the smallest sulfide droplets (Fig. 4c, 7a, Supplementary Tables S3-S5).

*5.3. Factors of silicate-sulfide immiscibility in the Tolbachik magmas*

Broadly correlated abundances of sulfur and chlorine in most sulfide-free silicate melt inclusions (0.1-0.35 wt% S and 0.05 - 0.14 wt% Cl) form a trend controlled by both crystallization and degassing (Fig. 3; Kamenetsky et al., 2017). The maximum concentrations of 0.35 wt% S and 0.14 wt% Cl measured in such MI can be regarded as concentrations of these volatiles in the melt at pressure and temperature of entrapment (< 5 kbar and <1230 °C; Kamenetsky et al., 2017), with the degassing trend reflecting magma decompression. However, a few analyzed silicate glasses that directly associate with sulfides (Figs. 5a, c, d) and those present as individual inclusions in olivine containing sulfide swarms (Fig. 4a-f), are significantly enriched in sulfur (0.5 – 1.1 wt% S, Fig. 3) and even contain anhydrite (Figs. 5c, d; Kamenetsky et al., 2017). In general, the sulfur content in the melt inclusions from the 1941 Tolbachik basalt are 2-3 times higher than in any measured melt inclusions from other Kamchatka rocks (e.g. Portnyagin et al., 2007b). Although the CaO contents and $CaO/Al_2O_3$ in the studied melt inclusions are somewhat high for mantle-derived melts

(Kamenetsky et al., 2017), in this case sulfur is the only volatile element close to or in excess of the maximum abundance measured in island arc magmas (Wallace and Edmonds, 2011).

Available modelling predicts that sulfur content at sulfide saturation (SCSS) in silicate melts depends on temperature, pressure, $fO_2$ and melt composition. Most models demonstrate that the SCSS correlates positively with temperature and oxygen fugacity and negatively with pressure. However, the effects of melt composition on SCSS values are still controversial. For example, 100–200 ppm Ni the melt may result in 1.5-2 fold decrease of SCSS (Ariskin et al., 2013), whereas the experimental model by Smythe et al. (2017) calculates even larger decrease of SCSS of up to an order of magnitude in the presence of several hundred ppm Ni and Cu. Unfortunately, this model is hardly applicable to arc magmas, because the experiments were conducted for anhydrous melts at deep mantle P-T conditions (1400-2160 °C, 1.5-24 GPa, and highly reduced conditions). Other models that are based on experiments with $H_2O$-saturated basaltic melts (Fortin et al., 2015; Liu et al., 2007) may have opposite conclusions on effects of $H_2O$ on SCSS and do not take oxygen fugacity into account. The model by Li and Ripley (2009) estimates sulfur content at sulfide or anhydrite saturation, but have limited application to melts where sulfide and sulfate coexist. The role of oxygen fugacity in governing SCSS has been accounted for by Jugo et al. (2010) as

$$SCSS = [S^{2-}]*(1+ 10\text{^}(2*\Delta QFM-2.1))$$

According to this model moderately oxidized Tolbachik melts (i.e. QFM +1…+1.5, Fig. 9; Kamenetsky et al., 2017) may achieve sulfide saturation at ~ 0.25 to 1.2 wt% total sulfur while $fO_2$ increases from QFM +1 to QFM +1.5 (Fig. 10). However, some other models (e.g. Ariskin et al., 2013; Jugo, 2009) predict lesser dependence of SCSS on $fO_2$ at the conditions of interest (~ 0.2-0.4 wt% total S; Fig. 10). Thus, as high S abundances in the Tolbachik melts (Fig. 3; Kamenetsky et al., 2017) appear to be a critical factor responsible for sulfide saturation. As only small proportion (<0.6%) of olivine phenocrysts record sulfide immiscibility, we are confident that common, although still elevated, abundances of S in the melt (~ 0.2-0.4 wt%) were not sufficient for sulfide saturation. On the other hand, the rarity of olivine with sulfide globules and melt inclusions containing anhydrite and extremely S-rich (Fig. 3-5) points to extraordinary conditions causing sulfide saturation and requirement of additional sulfur to match an exponential increase of SCSS in a narrow range of $fO_2$ (Fig. 10; Jugo et al., 2010).

*5.4. Distribution of sulfide melts in magmatic reservoir*

Olivine can entrap silicate melt as well as other liquid (e.g. sulfide melt), solid particles and fluid bubbles dispersed in magmas. The local character of sulfur enrichment and related sulfide immiscibility in the Tolbachik magma can be deduced from the sulfur abundances in melt inclusions and statistical parameters of sulfide globules. We consider that more than 200,000 examined olivine crystals are representative of the magma reservoir. Less than 1% of olivine phenocrysts contain sulfides, with several globules and swarms of globules more common than single globules. Similarly, only a few melt inclusions are characterized by anomalously high sulfur contents (> 0.5 wt%, Fig. 3, Supplementary Fig. S3) and/or may contain anhydrite (Fig. 5c, d), whereas most melt inclusions contain 0.3-0.35 wt% S or less (Kamenetsky et al., 2017). Such heterogeneous sulfur/sulfate/sulfide distribution suggests very specific conditions in terms of chemical (e.g. elevated sulfur content and related $S^{2-}$ super-saturation) and spatial conditions pertinent to volumes of melt that may undergo sulfide immiscibility.

In a first approximation, settling olivine grains, formed during fractional crystallization of mafic magma are more or less uniformly distributed within a cooling magma chamber (e.g. Hawkesworth et al., 2000 and references therein). Therefore, growing and settling olivine crystals can serve as “probes”, randomly entrapping sulfide droplets and melt inclusions throughout the whole magmatic reservoir and delivering them intact to the surface. According to Stokes' law, the settling velocity of a particle V is directly proportional to the density difference and increases as the square of the particle size R:

$$V = \frac{2}{9}\frac{(\rho_p - \rho_f)}{\mu} g R^2$$

where $\rho_p$ and $\rho_f$ are the mass densities of a particle and fluid, respectively, and $g$ the gravitational acceleration. Density difference between olivine (3.2 g/cm$^3$) and melt (2.8 g/cm$^3$) is around 0.4 g/cm$^3$ and density difference between sulfide (4.8 g/cm$^3$) and silicate melt is ~ 2 g/cm$^3$, which is five times higher. However, the average size of olivine crystals (~1 mm) is 1.5-3 orders of magnitude larger than majority of sulfide droplets (1-30 μm), which eventually results in overwhelming differences (3-5 orders of magnitude) in settling velocities of olivine crystals and sulfide droplets. Therefore, olivine crystals that descend through a parcel of the sulfide super-saturated melt may incorporate a large number of sulfide globules along growth planes and fractures (Fig. 4). The rest of the magma (> 99% of the total volume in our study) with 'conventional' sulfur abundances remains undersaturated in sulfide and produces sulfide-free olivine phenocrysts.

## 6. Conclusions

1. Our new data on sulfides in primitive arc magmas from the Tolbachik volcano (Kamchatka) provide a rare view of early immiscible sulfide melts, which previously were only considered theoretically or experimentally. In this volcanic suite even the smallest sulfide droplets proved to be Cu- and/or Ni-rich. The studied sulfide globules, as well as the host magnesian olivine, demonstrate substantial variability in Cu and Ni, likely caused by magma heterogeneity.

2. Low degree of sulfide supersaturation could cause diffusion equilibration of growing sulfide globules with relatively large volumes of silicate melt (high apparent R-factor) that ensured high concentrations of Cu and especially Ni even in the earliest micron-sized globules.

3. Sulfide segregation occurred at relatively high $fO_2$ = QFM +1…+1.5 due to high total sulfur ~ 1 wt%, which likely originated from some external source. These observations may be important in further development of a model for the formation of magmatic sulfide deposits.

4. This study is a novel insight into deeper level processes, indicating sulfide saturation and silicate-sulfide melt immiscibility early in the history of oxidized arc basalts, which further implies that it is possible to form sulfide deposits at deeper levels of magmatic arcs.

## Acknowledgements

We are indebted to Vasilii Yaschuk for help in collecting samples and Maya Kamenetsky for sample preparation. Insightful reviews of the earlier versions of this manuscript by Andy Tomkins, Pedro J. Jugo, Chusi Li and Edward M. Ripley are greatly appreciated. We thank three anonymous reviewers and guest editor Kate Kiseeva for careful comments. This study was supported by the Russian Science Foundation grant #16-17-10145.

## References

Ackermand, D., Hekinian, R., Stoffers, P., 1998. Magmatic sulfides and oxides in volcanic rocks from the Pitcairn hotspot (South Pacific). Mineral. Petrol., 61: 149-162.

Ariskin, A.A., Danyushevsky, L.V., Bychkov, K.A., McNeill, A.W., Barmina, G.S., Nikolaev, G.S., 2013. Modeling solubility of Fe-Ni sulfides in basaltic magmas: The effect of nickel. Econ. Geol., 108: 1983-2003.

Barnes, S.J., Godel, B., Gurer, D., Brenan, J.M., Robertson, J., Paterson, D., 2013. Sulfide-olivine Fe-Ni exchange and the origin of anomalously Ni rich magmatic sulfides. Econ. Geol., 108: 1971-1982.

Belousov, A., Belousova, M., Edwards, B., Volynets, A., Melnikov, D., 2015. Overview of the precursors and dynamics of the 2012-13 basaltic fissure eruption of Tolbachik Volcano, Kamchatka, Russia. J. Volcanol. Geotherm. Res., 307: 22-37.

Braitseva, O.A., Melekestsev, I.V., Flerov, G.B., Ponomareva, V.V., Sulerzhitsky, L.D., Litasova, S.N., 1984. Holocene volcanism of the Tolbachik regional zone of cinder cones. In: Fedotov, S.A. (Ed.), The Great Tolbachik Fissure Eruption, Kamchatka, 1975-1976. Nauka, Moscow, pp. 177-209 (in Russian).

Churikova, T.G., Gordeychik, B.N., Edwards, B.R., Ponomareva, V.V., Zelenin, E.A., 2015a. The Tolbachik volcanic massif: A review of the petrology, volcanology and eruption history prior to the 2012-2013 eruption. J. Volcanol. Geotherm. Res., 307: 3-21.

Churikova, T.G., Gordeychik, B.N., Iwamori, H., Nakamura, H., Ishizuka, O., Nishizawa, T., Haraguchi, S., Miyazaki, T., Vaglarov, B.S., 2015b. Petrological and geochemical evolution of the Tolbachik volcanic massif, Kamchatka, Russia. J. Volcanol. Geotherm. Res., 307: 156-181.

Czamanske, G.K., Moore, J.G., 1977. Composition and phase chemistry of sulfide globules in basalt from the Mid-Atlantic ridge rift valley near 37° N lat. Geol. Soc. Am. Bull., 88: 587-599.

DeMets, C., Gordon, R.G., Argus, D.F., Stein, S., 1990. Current plate motions. Geophys. J. Int., 101: 425-478.

Evans, K., Elburg, M.A., Kamenetsky, V.S., 2012. The oxidation state of sub-arc mantle. Geology, 40: 783–786.

Fleet, M.E., Stone, W.E., 1990. Nickeliferous sulfides in xenoliths, olivine megacrysts and basaltic glass. Contrib. Mineral. Petrol., 105: 629-636.

Flerov, G.B., Andreev, V.N., Budnikov, V.A., Tsyurupa, A.I., 1984. Petrology of the eruption products. In: Fedotov, S.A. (Ed.), The Great Tolbachik Fissure Eruption, Kamchatka, 1975-1976. Nauka, Moscow, pp. 223-284 (in Russian).

Fortin, M.-A., Riddle, J., Desjardins-Langlais, Y., Baker, D.R., 2015. The effect of water on the sulfur concentration at sulfide saturation (SCSS) in natural melts. Geochim. Cosmochim. Acta, 160: 100-116.

Francis, R.D., 1990. Sulfide globules in mid-ocean ridge basalts (MORB), and the effect of oxygen abundance in Fe-S-O liquids on the ability of those liquids to partition metals from MORB and komatiite magmas. Chem. Geol., 85: 199-213.

Gorbatov, A., Kostoglodov, V., Suárez, G., Gordeev, E., 1997. Seismicity and structure of the Kamchatka subduction zone. Journal of Geophysical Research B: Solid Earth, 102: 17883-17898.

Gurenko, A.A., Poliakov, A.I., Kononkova, N.N., 1987. Immiscible sulfide segregations in minerals of early crystallization stages of basaltic rock series. Dokl. Akad. Nauk SSSR, 293: 439-443.

Hawkesworth, C.J., Blake, S., Evans, P., Hughes, R., MacDonald, R., Thomas, L.E., Turner, S.P., Zellmer, G., 2000. Time scales of crystal fractionation in magma chambers - Integrating physical, isotopic and geochemical perspectives. J. Petrol., 41: 991-1006.

Henley, R.W., King, P.L., Wykes, J.L., Renggli, C.J., Brink, F.J., Clark, D.A., Troitzsch, U., 2015. Porphyry copper deposit formation by sub-volcanic sulphur dioxide flux and chemisorption. Nat. Geosci., 8: 210-215.

Holwell, D.A., McDonald, I., Butler, I.B., 2011. Precious metal enrichment in the Platreef, Bushveld Complex, South Africa: Evidence from homogenized magmatic sulfide melt inclusions. Contrib. Mineral. Petrol., 161: 1011-1026.

Holzheid, A., 2010. Separation of sulfide melt droplets in sulfur saturated silicate liquids. Chem. Geol., 274: 127-135.

Humphreys, M.C.S., Brooker, R.A., Fraser, D.G., Burgisser, A., Mangan, M.T., McCammon, C.A., 2015. Coupled interactions between volatile activity and Fe oxidation state during arc crustal processes. J. Petrol., 56: 795–814.

Iwasaki, T., Levin, V., Nikulin, A., Iidaka, T., 2013. Constraints on the Moho in Japan and Kamchatka. Tectonophysics, 609: 184-201.

Jenner, F.E., O'Neill, H.S.C., Arculus, R.J., Mavrogenes, J.A., 2010. The magnetite crisis in the evolution of arc-related magmas and the initial concentration of Au, Ag and Cu. J. Petrol., 51: 2445-2464.

Jugo, P.J., 2009. Sulfur content at sulfide saturation in oxidized magmas. Geology, 37: 415-418.

Jugo, P.J., Luth, R.W., Richards, J.P., 2005a. Experimental data on the speciation of sulfur as a function of oxygen fugacity in basaltic melts. Geochim. Cosmochim. Acta, 69: 497-503.

Jugo, P.J., Luth, R.W., Richards, J.P., 2005b. An experimental study of the sulfur content in basaltic melts saturated with immiscible sulfide or sulfate liquids at 1300 ºC and 1.0 GPa. J. Petrol., 46: 783-798.

Jugo, P.J., Wilke, M., Botcharnikov, R.E., 2010. Sulfur K-edge XANES analysis of natural and synthetic basaltic glasses: Implications for S speciation and S content as function of oxygen fugacity. Geochim. Cosmochim. Acta, 74: 5926-5938.

Kamenetsky, V.S., Maas, R., Fonseca, R.O.C., Ballhaus, C., Heuser, A., Brauns, M., Norman, M.D., Woodhead, J.D., Rodemann, T., Kuzmin, D.V., Bonatti, E., 2013. Noble metals potential of sulfide-saturated melts from the subcontinental lithosphere. Geology, 41: 575-578.

Kamenetsky, V.S., Zelenski, M., Gurenko, A., Portnyagin, M., Ehrig, K., Kamenetsky, M., Churikova, T., Feig, S., 2017. Silicate-sulfide liquid immiscibility in modern arc basalt (Tolbachik volcano, Kamchatka): Part II. Composition, liquidus assemblage and fractionation of the silicate melt. Chem. Geol., (this volume).

Keith, J.D., Whitney, J.A., Hattori, K., Ballantyne, G.H., Christiansen, E.H., Barr, D.L., Cannan, T.M., Hook, C.J., 1997. The role of magmatic sulfides and mafic alkaline magmas in the Bingham and Tintic mining districts, Utah. J. Petrol., 38: 1679-1690.

Larocque, A.C.L., Stimac, J.A., Keith, J.D., Huminicki, M.A.E., 2000. Evidence for open-system behavior in immiscible Fe-S-O liquids in silicate magmas: Implications for contributions of metals and sulfur to ore-forming fluids. Can. Mineral., 38: 1233-1249.

Li, C.S., Ripley, E.M., 2005. Empirical equations to predict the sulfur content of mafic magmas at sulfide saturation and applications to magmatic sulfide deposits. Mineral. Deposita, 40: 218-230.

Li, C.S., Ripley, E.M., 2009. Sulfur contents at sulfide-liquid or anhydrite saturation in silicate melts: Empirical equations and example applications. Econ. Geol., 104: 405-412.

Liu, Y.N., Samaha, N.T., Baker, D.R., 2007. Sulfur concentration at sulfide saturation (SCSS) in magmatic silicate melts. Geochim. Cosmochim. Acta, 71: 1783-1799.

Mathez, E.A., 1976. Sulfur solubility and magmatic sulfides in submarine basalt glass. J. Geophys. Res., 81: 4269-4276.

Matjuschkin, V., Blundy, J.D., Brooker, R.A., 2016. The effect of pressure on sulphur speciation in mid-to deep-crustal arc magmas and implications for the formation of porphyry copper deposits. Contrib. Mineral. Petrol., 171.

Mavrogenes, J., Blundy, J., 2017. Crustal sequestration of magmatic sulfur dioxide. Geology, 10.1130/G38555.1.

Mungall, J.E., 2002. Kinetic controls on the partitioning of trace elements between silicate and sulfide liquids. J. Petrol., 43: 749-768.

Nadeau, O., Williams-Jones, A.E., Stix, J., 2010. Sulphide magma as a source of metals in arc-related magmatic hydrothermal ore fluids. Nat. Geosci., 3: 501-505.

Naldrett, A.J., 2004. Magmatic Sulfide Deposits: Geology, geochemistry and exploration. Springer-Verlag, Berlin Heidelberg.

Namur, O., Charlier, B., Holtz, F., Cartier, C., McCammon, C., 2016. Sulfur solubility in reduced mafic silicate melts: Implications for the speciation and distribution of sulfur on Mercury. Earth Planet. Sci. Lett., 448: 102-114.

O'Neill, H.S.C., Mavrogenes, J.A., 2002. The sulfide capacity and the sulfur content at sulfide saturation of silicate melts at 1400 ºC and 1 bar. J. Petrol., 43: 1049-1087.

Patten, C., Barnes, S.J., Mathez, E.A., 2012. Textural variations in MORB sulfide droplets due to differences in crystallization history. Can. Mineral., 50: 675-692.

Peach, C.L., Mathez, E.A., 1993. Sulfide melt-silicate melt distribution coefficients for nickel and iron and implications for the distribution of other chalcophile elements. Geochim. Cosmochim. Acta, 57: 3013-3021.

Peach, C.L., Mathez, E.A., Keays, R.R., 1990. Sulfide melt-silicate melt distribution coefficients for noble metals and other chalcophile elements as deduced from MORB: Implication for partial melting. Geochim. Cosmochim. Acta, 54: 3379-3389.

Piip, B.I., 1946. The activity of the Tolbachik volcano (January 1941). Bulletin of the volcanological station, 12: 70–73 (In Russian).

Portnyagin, M., Bindeman, I., Hoernle, K., Hauff, F., 2007a. Geochemistry of primitive lavas of the Central Kamchatka Depression: magma generation at the edge of the Pacific Plate. In: Eichelberger, J., Gordeev, E., Izbekov, P., Kasahara, M., Lees, J. (Eds.), Volcanism and subduction: the Kamchatka region, pp. 199-239.

Portnyagin, M., Duggen, S., Hauff, F., Mironov, N., Bindeman, I., Thirlwall, M., Hoernle, K., 2015. Geochemistry of the late Holocene rocks from the Tolbachik volcanic field, Kamchatka: Quantitative modelling of subduction-related open magmatic systems. J. Volcanol. Geotherm. Res., 307: 133-155.

Portnyagin, M., Hoernle, K., Avdeiko, G., Hauff, F., Werner, R., Bindeman, I., Uspensky, V., Garbe-Schönberg, D., 2005. Transition from arc to oceanic magmatism at the Kamchatka-Aleutian junction. Geology, 33: 25-28.

Portnyagin, M., Hoernle, K., Plechov, P., Mironov, N., Khubunaya, S., 2007b. Constraints on mantle melting and composition and nature of slab components in volcanic arcs from volatiles ($H_2O$, S, Cl, F) and trace elements in melt inclusions from the Kamchatka Arc. Earth Planet. Sci. Lett., 255: 53-69.

Richards, J.P., 2015. The oxidation state, and sulfur and Cu contents of arc magmas: implications for metallogeny. Lithos, 233: 27-45.

Smythe, D.J., Wood, B.J., Kiseeva, E.S., 2017. The S content of silicate melts at sulfide saturation: New experiments and a model incorporating the effects of sulfide composition. Am. Mineral., 102: 795-803.

Steblov, G.M., Kogan, M.G., King, R.W., Scholz, C.H., Bürgmann, R., Frolov, D.I., 2003. Imprint of the North American plate in Siberia revealed by GPS. Geophys. Res. Lett., 30: 10.1029/2003GL017805.

Stone, W.E., Fleet, M.E., 1991. Nickel-copper sulfides from the 1959 eruption of Kilauea Volcano, Hawaii: Contrasting compositions and phase relations in eruption pumice and Kilauea Iki lava lake. Am. Mineral., 76: 1363-1372.

Tomkins, A.G., Rebryna, K.C., Weinberg, R.F., Schaefer, B.F., 2012. Magmatic sulfide formation by reduction of oxidized arc basalt. J. Petrol., 53: 1537-1567.

Wallace, P.J., Edmonds, M., 2011. The sulfur budget in magmas: Evidence from melt inclusions, submarine glasses, and volcanic gas emissions, Reviews in Mineralogy and Geochemistry, pp. 215-246.

Wilkinson, J.J., 2013. Triggers for the formation of porphyry ore deposits in magmatic arcs. Nat. Geosci., 6: 917-925.

Wykes, J.L., O'Neill, H.S.C., Mavrogenes, J.A., 2014. The effect of FeO on the sulfur content at sulfide saturation (SCSS) and the selenium content at selenide saturation of silicate melts. J. Petrol., 56: 1407-1424.

Zhang, Y., 2015. Toward a quantitative model for the formation of gravitational magmatic sulfide deposits. Chem. Geol., 391: 56-73.

Figure captions

Fig. 1. Location of Tolbachik volcano and the 1941 and Mt. 1004 eruptive cones with the adjacent lava and scoria fields.

Fig. 2. Typical zoned olivine phenocryst with core $Fo_{90}$ to rim $Fo_{84}$ compositional variations (a) and abundances of chalcophile metals in sulfide-free (open circles) and sulfide-bearing (grey circles) olivine phenocrysts from the 1941 eruption basalt (b-d).

Fig. 3. Sulfur vs. chlorine contents of the groundmass glasses (1) and olivine-hosted silicate melt inclusions (2-6) from the 1941 eruption of Tolbachik. The majority of glass inclusions (homogenized in heating experiments (2) and naturally quenched (3)) are not associated with sulfide globules and/or anhydrite, and follow crystallization/degassing trends with sulphur not exceeding ~ 0.35 wt%. Some olivine-hosted inclusions of the silicate melt (4-6) contain anomalously high sulfur (> 0.4 wt% S) and are represented by clear glass (4), glass associated with sulfide globules (5) and partially devitrified melt associated with sulfide globules and anhydrite (6).

Fig. 4. Optical (transmitted and reflected light) microphotographs of the 1941 Tolbachik olivine hosting sulfide globules as “swarms” or “arrays” (a-d), along growth planes (f) and sulfide films wetting fractures (g).

Fig. 5. Typical associations of olivine-hosted sulfide globules with the silicate melt (a-d, h), fluid bubbles (a-d, g), clinopyroxene and anhydrite (c, d). A magnetite component (M) is often present within sulfide globules. Naturally quenched sulfide melt may appear as fine-grained (a, c-e) or inhomogeneous/multiphase (f). The heated and quenched sulfide melts are homogeneous (g) or have fine-grained texture (h). The labels denote glass (G), fluid bubbles (B), anhydrite (A), clinopyroxene (Px), Fe-Ni-S monosulfide solid solution (MSS) and Fe-Cu-S intermediate solid solution (ISS), chalcopyrite (ccp), cubanite (cb) and mixed Cu-Ni-bearing (Cu+Ni) compositions. The photos are made using transmitted-reflected light (a), transmitted light (b), reflected light (e-h) and backscattered electrons (c, d).

Fig. 6. Correspondence between compositions of sulfide globules analyzed on exposed surfaces by energy-dispersive spectroscopy (scanning electron microscope, ESEM EDS) and by the volume ablation using laser-ablation ICPMS.

Fig. 7. Compositional variability of sulfide globules: (a) naturally quenched from the 1941 and Mt. 1004 cones of the Tolbachik volcano; (b) reheated and quenched from the 1941 cone in

comparison to small (<10 μm) globules from "swarms (e.g. Fig. 4 a-d); (c) in mid-ocean riftogenic basaltic glasses (MORB; Francis, 1990), in glasses and olivine phenocrysts from the Kilauea volcano, Hawaii (OIB, Fleet and Stone, 1990) and in Cr-spinel from Platreef, Bushveld (Holwell et al., 2011).

Fig. 8. Relationships between compositions of olivine and olivine-hosted sulfide globules in terms of chalcophile elements (Ni and Cu).

Fig. 9. Relationships between Ni content in sulfide melts and Ni-Fe exchange coefficients $K_D$ for olivine-sulfide pairs in the Tolbachik samples. Most sulfides, irrespective of their Cu contents, formed at the same oxygen fugacity (~ QFM+1…+1.5), based on established dependence between $K_D$ and $fO_2$ (Barnes et al., 2013).

Fig. 10. Sulfur content at sulfide saturation (SCSS) vs. oxygen fugacity as predicted by different models: 1 – Jugo (2009); 2 – Jugo et al. (2010); 3 and 4 –at 0 ppm and 200 Ni, respectively by Ariskin et al. (2013). Total sulfur contents of Tolbachik melt inclusions in sulfide-free and sulfide-bearing olivine are from Fig. 3 and Kamenetsky et al. (2017).

**Figure 1**

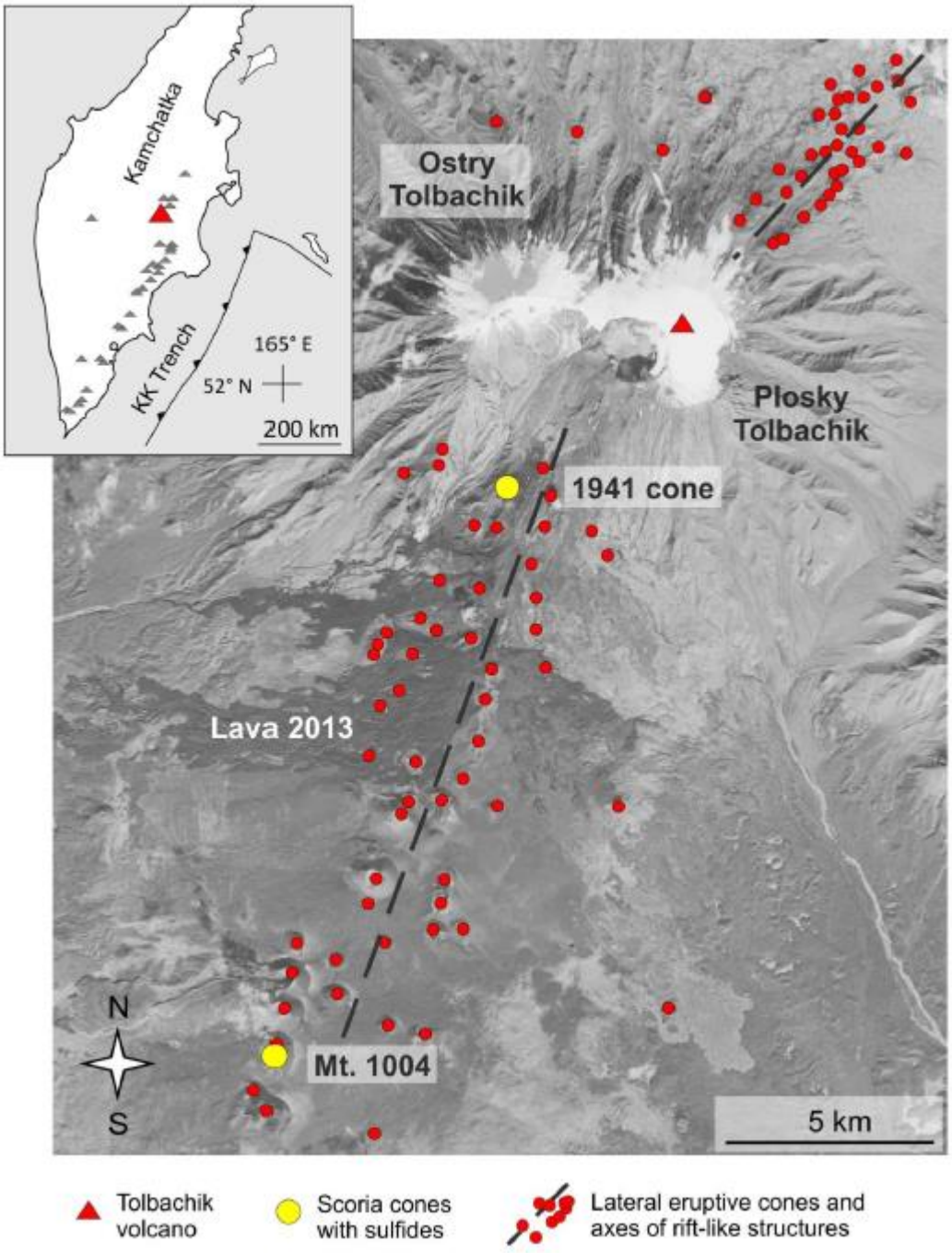

**Figure 2**

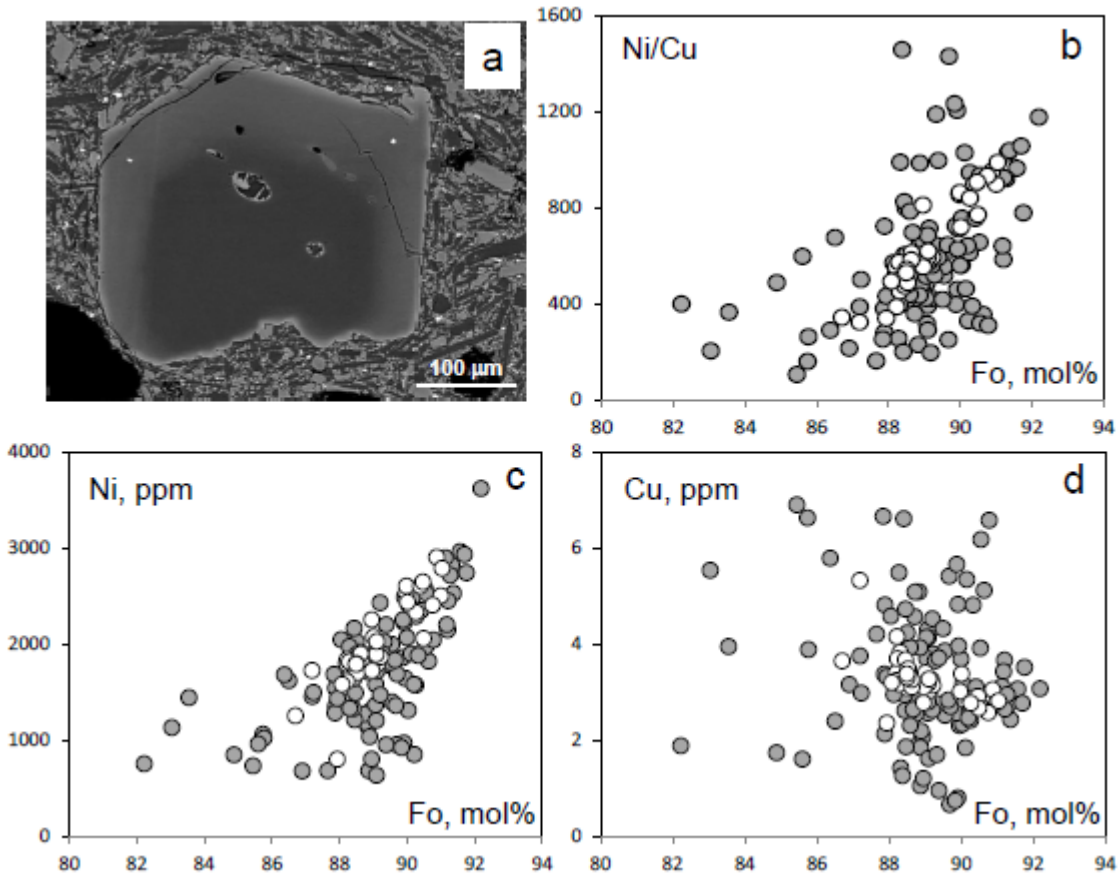

**Figure 3**

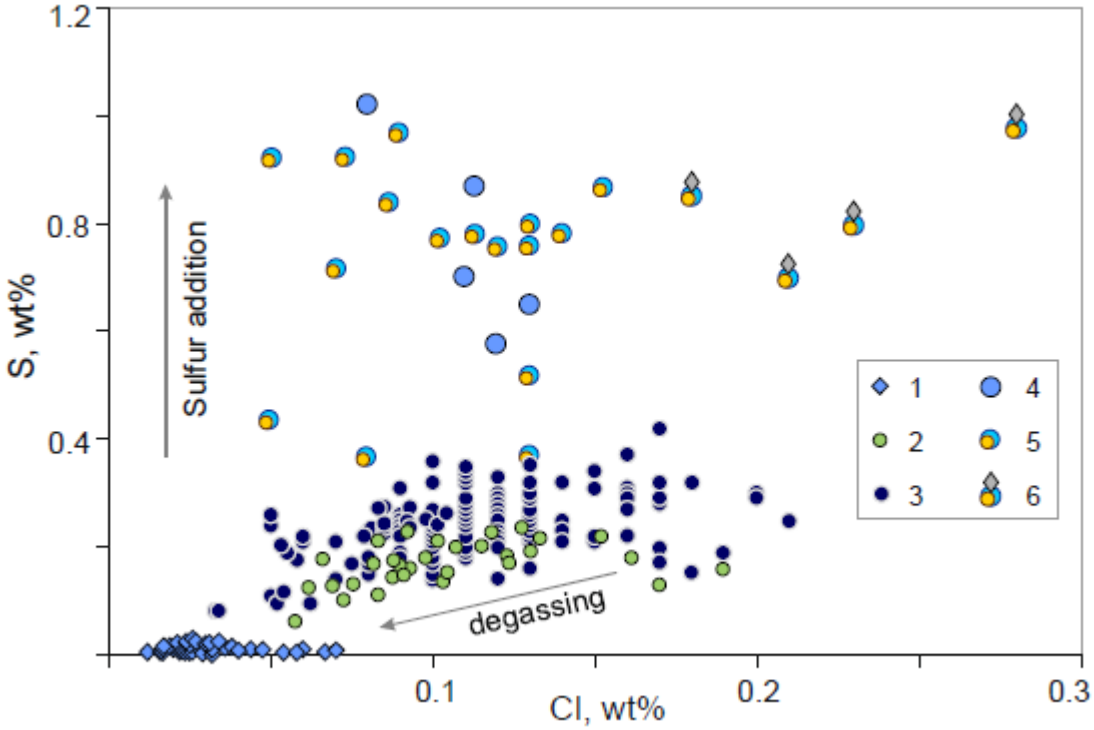

**Figure 4**

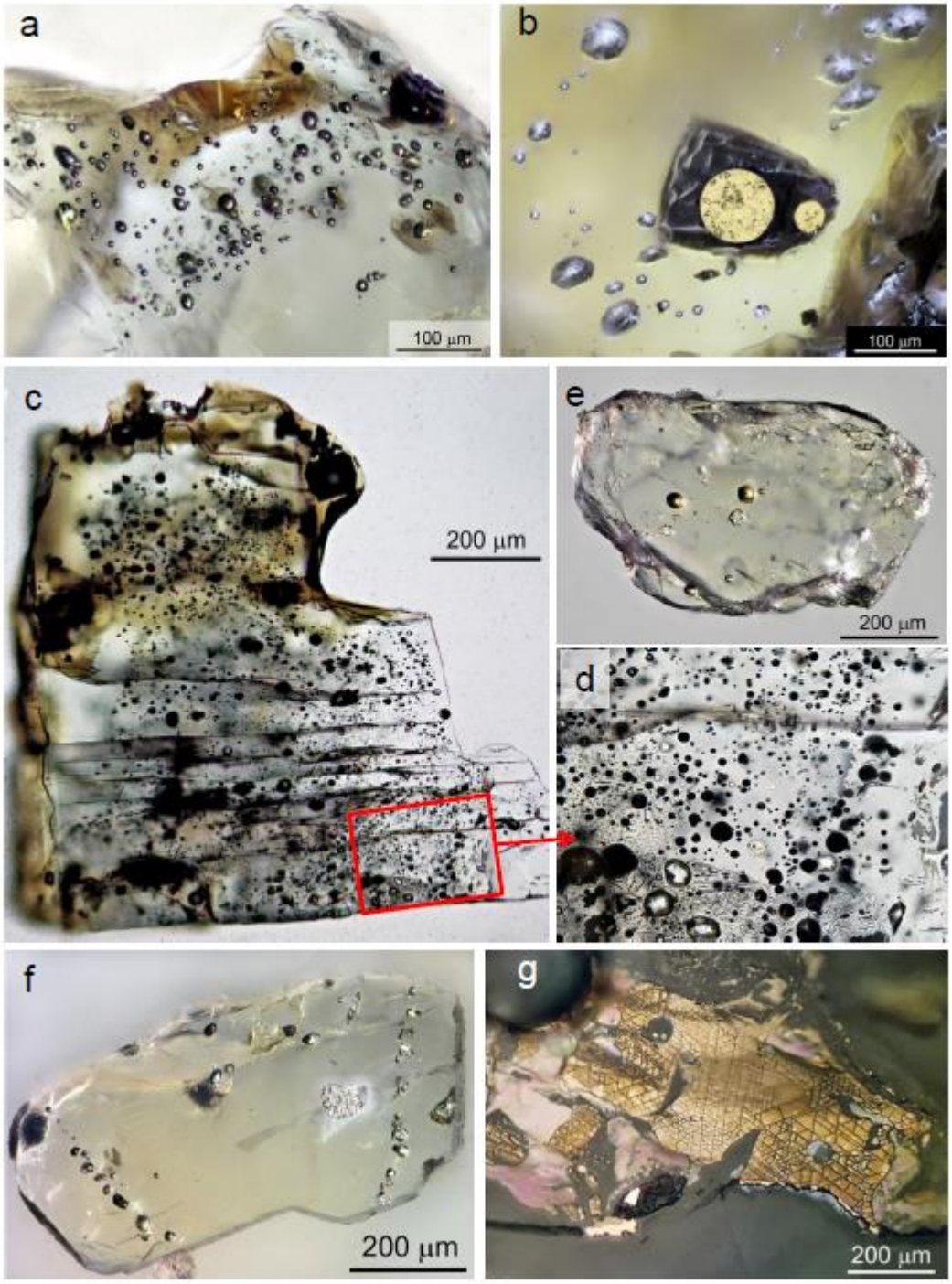

**Figure 5**

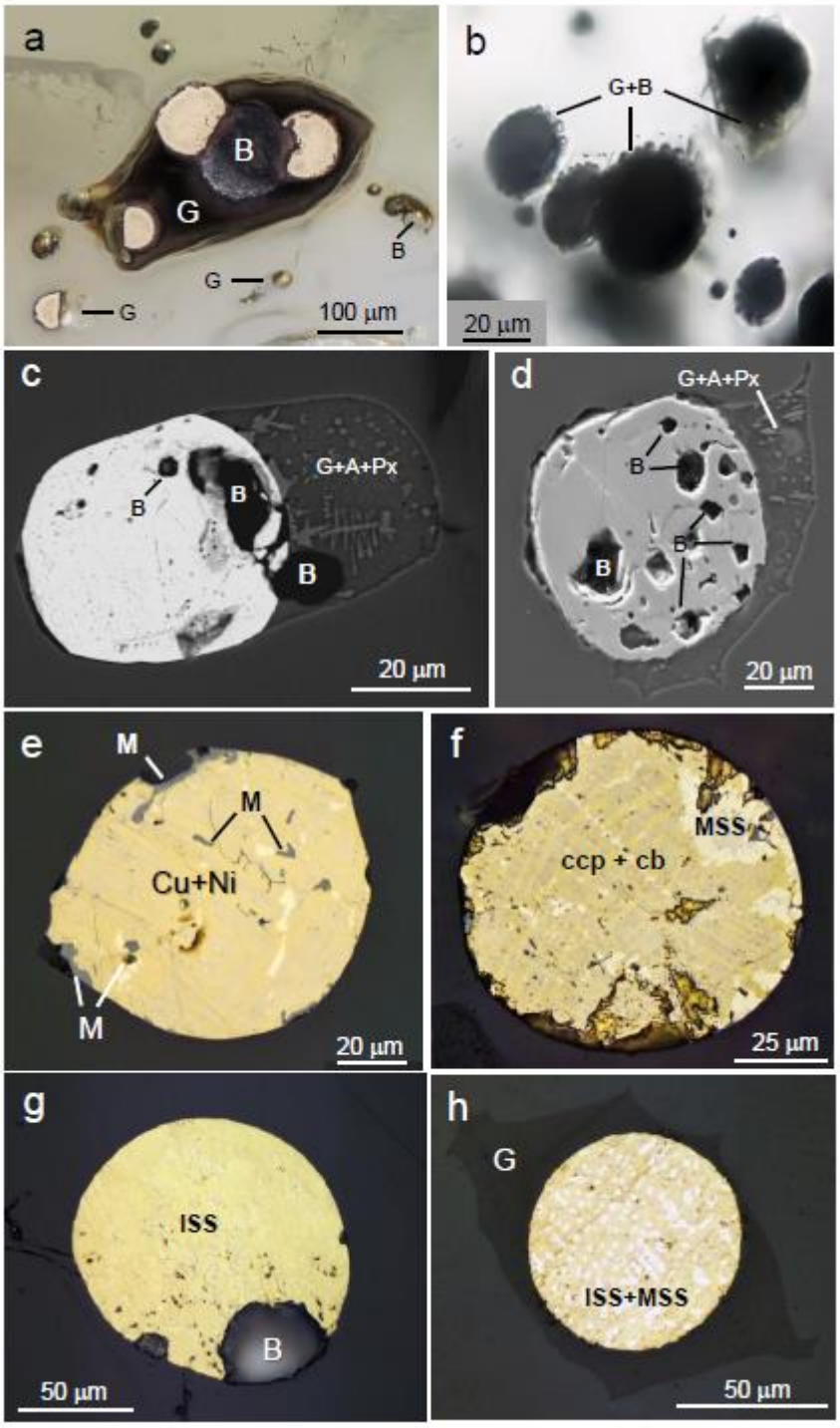

**Figure 6**

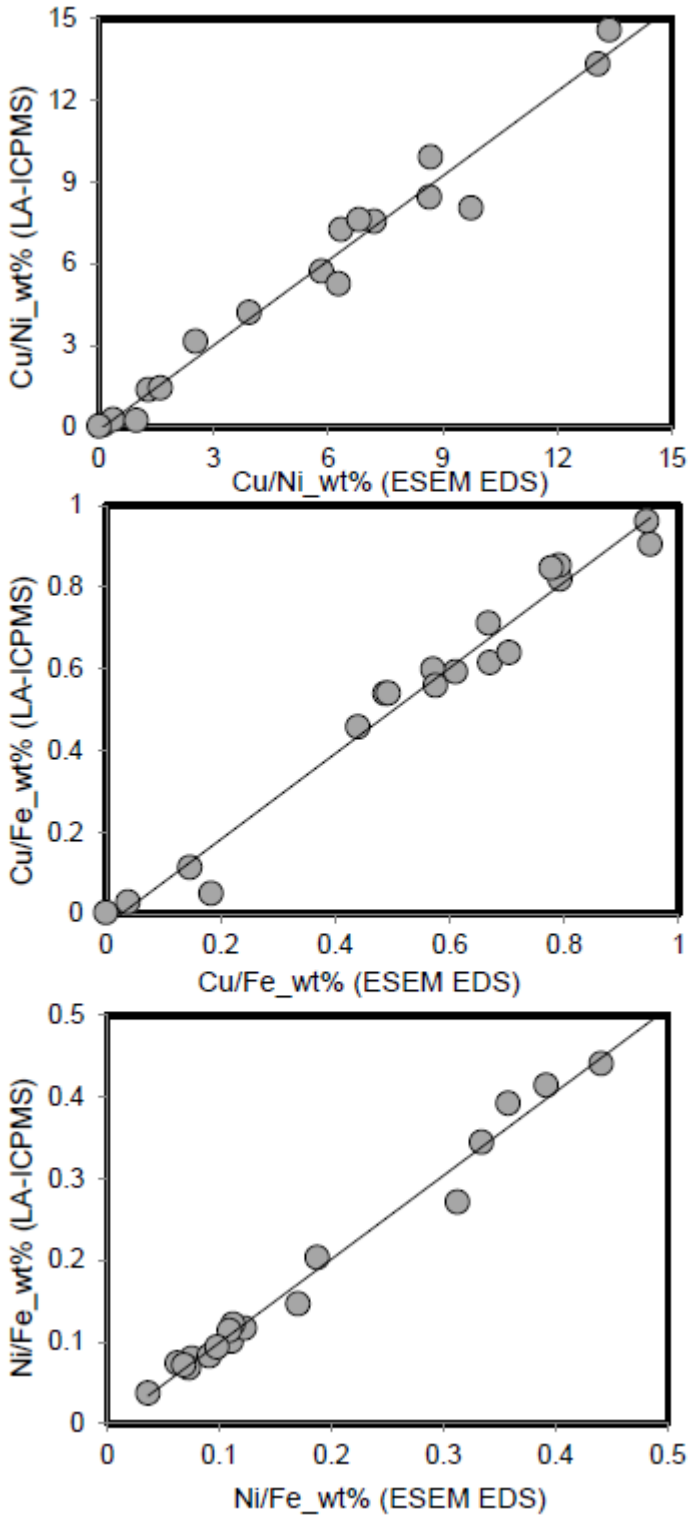

**Figure 7**

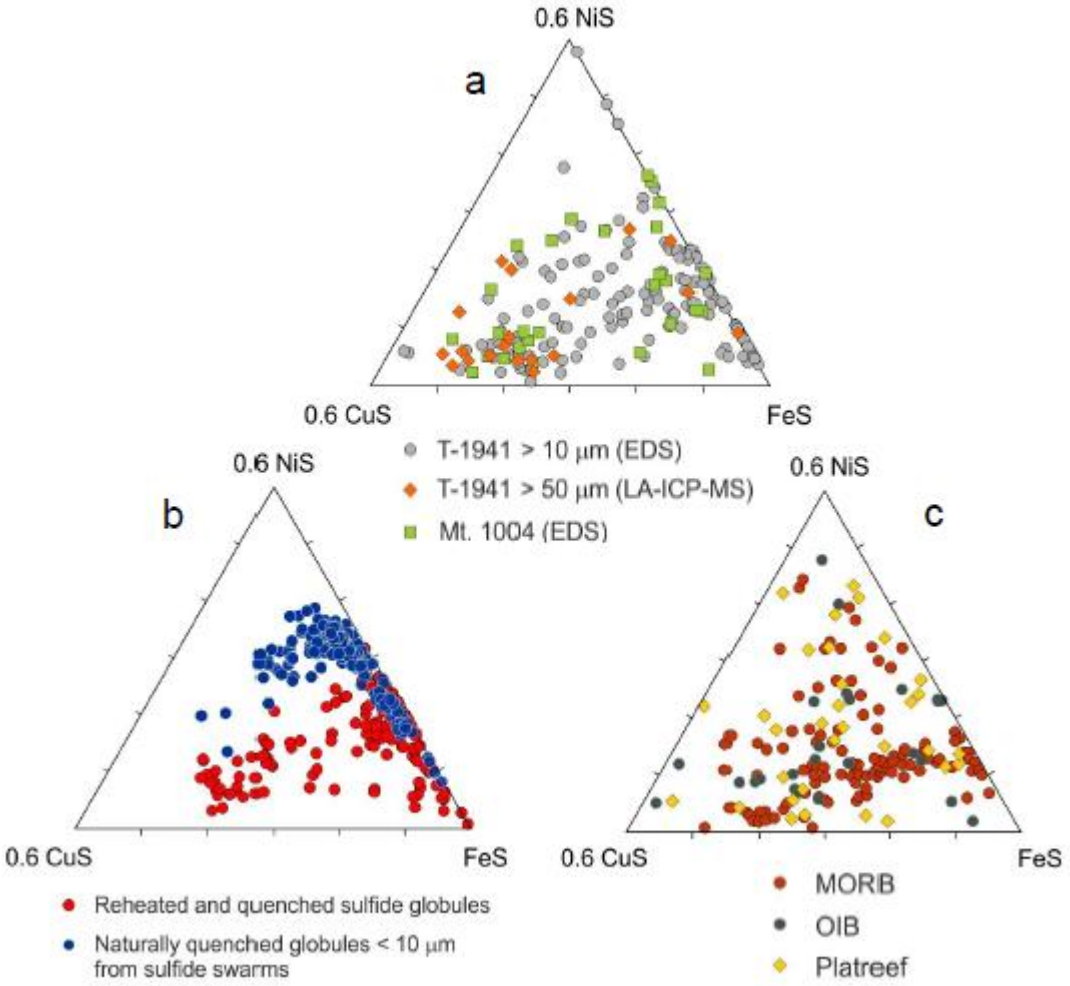

**Figure 8**

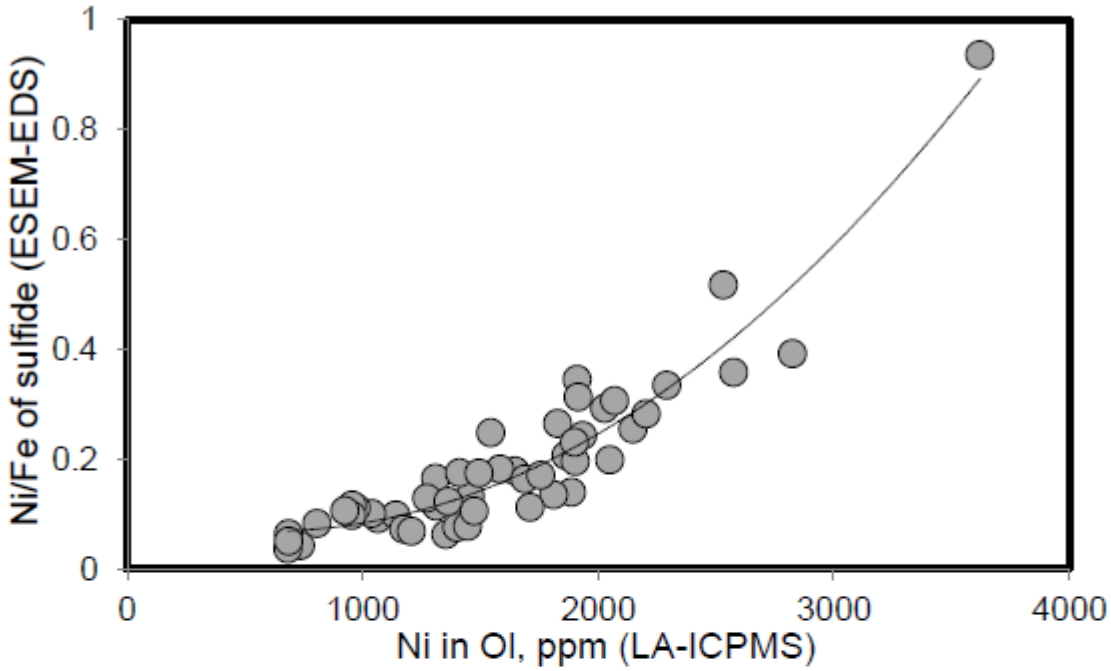


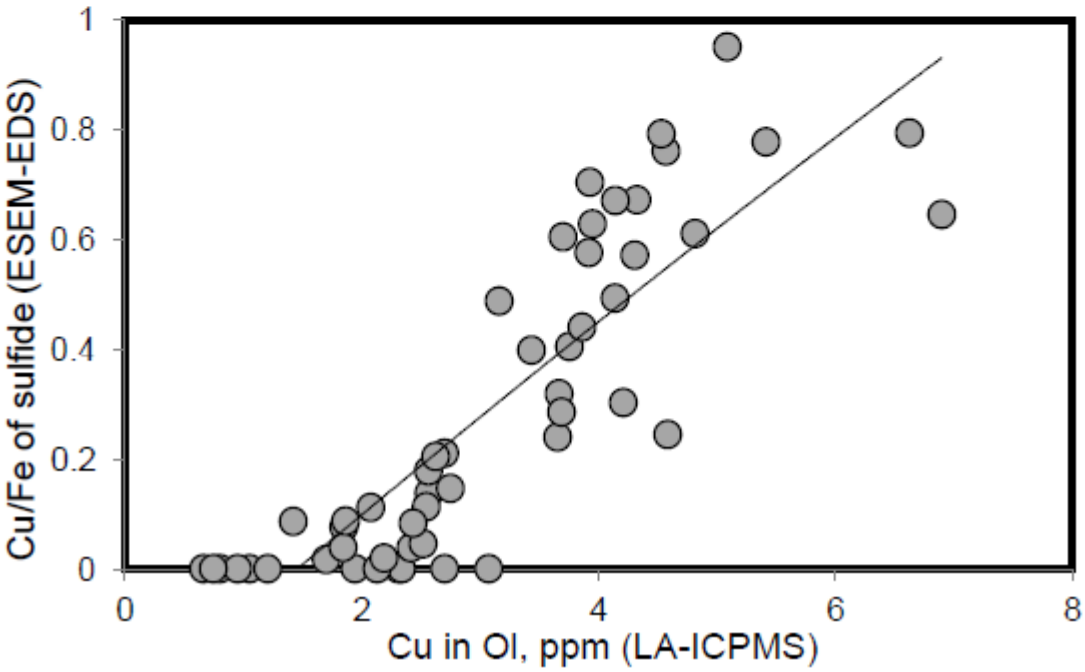

**Figure 9**

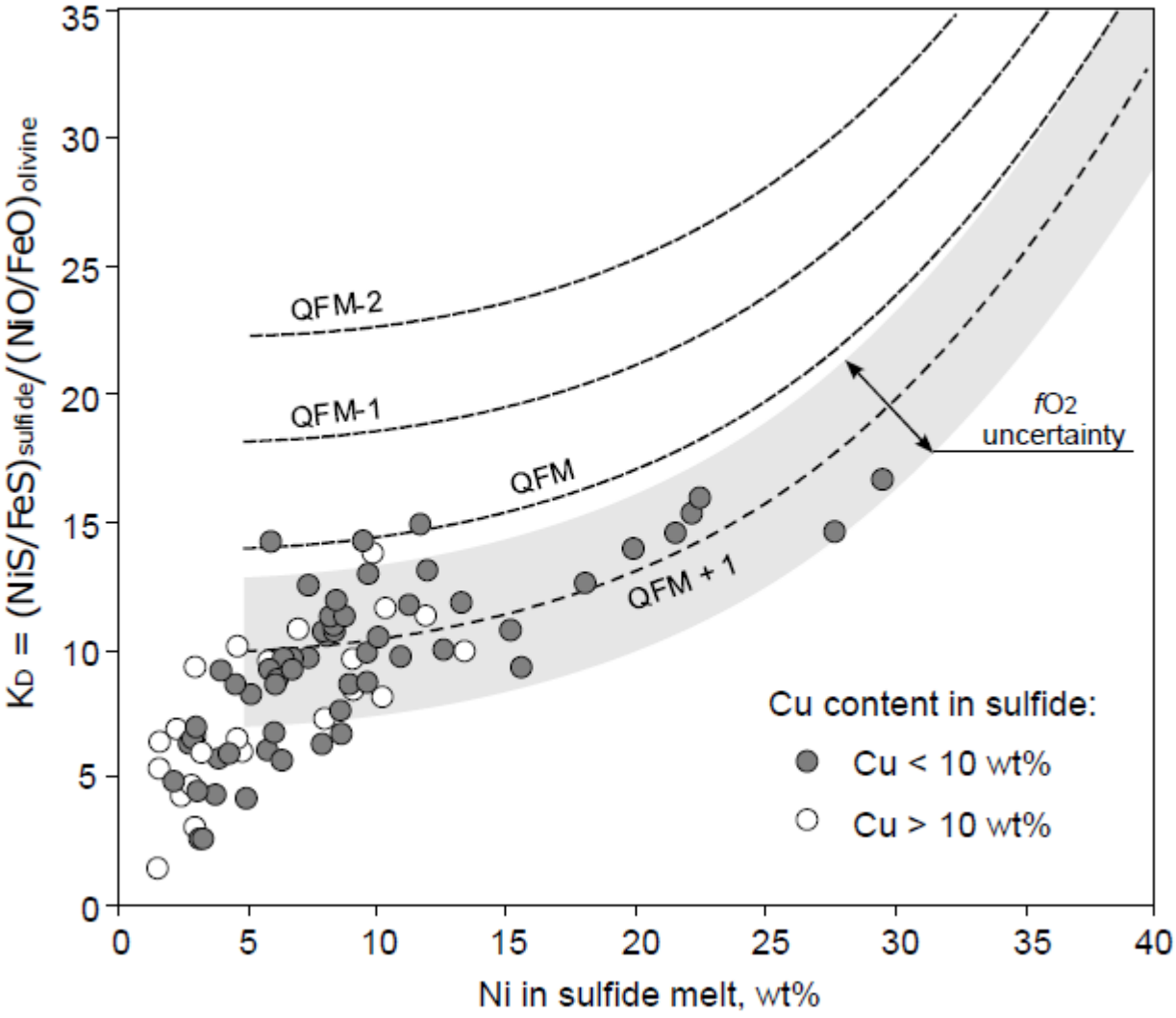

**Figure 10**